Computational Study of the Unimolecular Decomposition Pathways of Phenylperoxy Radical

Michael J. Fadden, Cynthia Barckholtz, and Christopher M. Hadad*

Department of Chemistry, The Ohio State University, Columbus, Ohio 43210

Received: November 10, 1999; In Final Form: February 7, 2000

The potential energy surface for the unimolecular decomposition of phenylperoxy radical has been explored using the B3LYP method. Several pathways were considered including the initial formation of the phenoxy, dioxiranyl, 1,2-dioxetanyl, 1,3-peroxy, and *p*-phenylquinone radicals. Transition states for all pathways on the potential energy surface are presented. At all temperatures studied ($T \leq 1250$ K), the energetically most favored pathway is the dioxiranyl pathway which leads to the formation of cyclopentadienyl radical and CO_2, pyranyl radical and CO, or an acyclic $C_6H_5O_2$ radical structure as products. The ring-opening reactions are very competitive with formation of CO and CO_2 as products.

Introduction

The reaction of phenyl radical with O_2 is of great importance in the study of combustion and atmospheric chemistry and has received much attention. The major product channel at intermediate and high temperatures has been reported to follow the path[1−3]

$$C_6H_5^{\bullet} + O_2 \rightarrow C_6H_5O^{\bullet} + O$$

$$C_6H_5O^{\bullet} \rightarrow C_5H_5^{\bullet} + CO$$

but controversy still exists over the exact mechanisms as current models still fail to accurately predict the experimental formation and concentrations of products at various temperatures from the combustion of benzene with oxygen.[4]

The relevance of phenylperoxy radical ($C_6H_5OO^{\bullet}$) as a viable intermediate at intermediate temperatures is also disputed. Benson theorized on thermochemical grounds that phenylperoxy radical would not be stable at temperatures above 433 K,[5] but it has been shown experimentally that, at temperatures as high as 473 K, $C_6H_5OO^{\bullet}$ can still be detected and the phenoxy radical ($C_6H_5O^{\bullet}$) is absent.[6] Therefore, $C_6H_5OO^{\bullet}$ cannot be discounted as an important intermediate of the reaction of phenyl radical with oxygen at low to intermediate temperatures.

Computational studies over the past decade have explored alternate pathways of the unimolecular decomposition of $C_6H_5OO^{\bullet}$ and have centered mainly on the formation of dioxiranyl and dioxetanyl intermediates which can then decompose to the cyclopentadienyl radical ($C_5H_5^{\bullet}$, $Cp^{\bullet}$) and CO or CO_2.[7,8] The dioxiranyl pathway was proposed by Carpenter on the basis of PM3 calculations.[7] Further analysis at the B3LYP/6-31G* level demonstrated the viability of the dioxiranyl pathway at low temperatures; however, we were unable at that time to provide a complete potential energy surface, including activation barriers, for the decomposition of aromatic peroxy radicals.[8] These previous studies suggested that other pathways may be competitive with the phenoxy radical pathway at intermediate temperatures ($T < 1000$ K).[7−8]

The vinyl radical and O_2 potential energy surface has been exhaustively studied by Carpenter[9] and Lin, Morokuma, and co-workers,[10] but larger, unsaturated radicals have been less well studied. However, there have been some computational studies relevant to phenyl radical oxidation.[11−14] For instance, the decomposition pathways for the phenoxy radical have been investigated.[11,12] Various $C_6H_5O_2$ isomers have been studied by Mebel and Lin,[13] and these authors also examined the O + $C_6H_5O^{\bullet}$ potential energy surface.[14] However, a quantitatively accurate comparison of the different pathways available to the phenylperoxy radical is still lacking. Some of the previous computational studies were completed via unrestricted Hartree−Fock-based methods, and spin contamination was significant. Lin, Morokuma, and co-workers have shown that density functional theory methods can be accurately applied to benzene reactions with hydrogen atoms.[15] We have also demonstrated that DFT methods, and the B3LYP functional in particular, can be accurately applied to aromatic radicals as spin contamination is not a significant problem.[8,16]

This paper is an extension of a previous computational study of the possible unimolecular decomposition pathways of $C_6H_5OO^{\bullet}$ at temperatures ranging from 273 to 2000 K.[8] Computationally, we now explore the phenoxy and dioxiranyl radical pathways as well as the 1,2-dioxetanyl, 1,3-peroxy, and *p*-phenylquinonyl radical pathways and provide energetics of the intermediates and transition states using the B3LYP density functional theory method.

Computational Methods

All geometry optimizations and vibrational frequency calculations were performed with Gaussian 94 and 98 at the Ohio Supercomputer Center.[17,18] The optimized geometries were calculated at the B3LYP/6-31G* hybrid density functional theory level, and single-point energies at these optimized geometries were determined at the B3LYP/6-311+G** level (using the scf=tight option).[19−22] All basis sets used six Cartesian *d* functions. Bauschlicher and Langhoff have shown that there is a small basis set effect in B3LYP calculations for oxygen-containing systems for determining C−H bond dissociation energies.[23] The B3LYP/6-311+G** single-point energies should compensate for such deficiencies.

* Corresponding author. Fax: (614) 292-1685. E-mail: hadad.1@osu.edu.

10.1021/jp993990n CCC: $19.00
Published on Web 03/11/2000

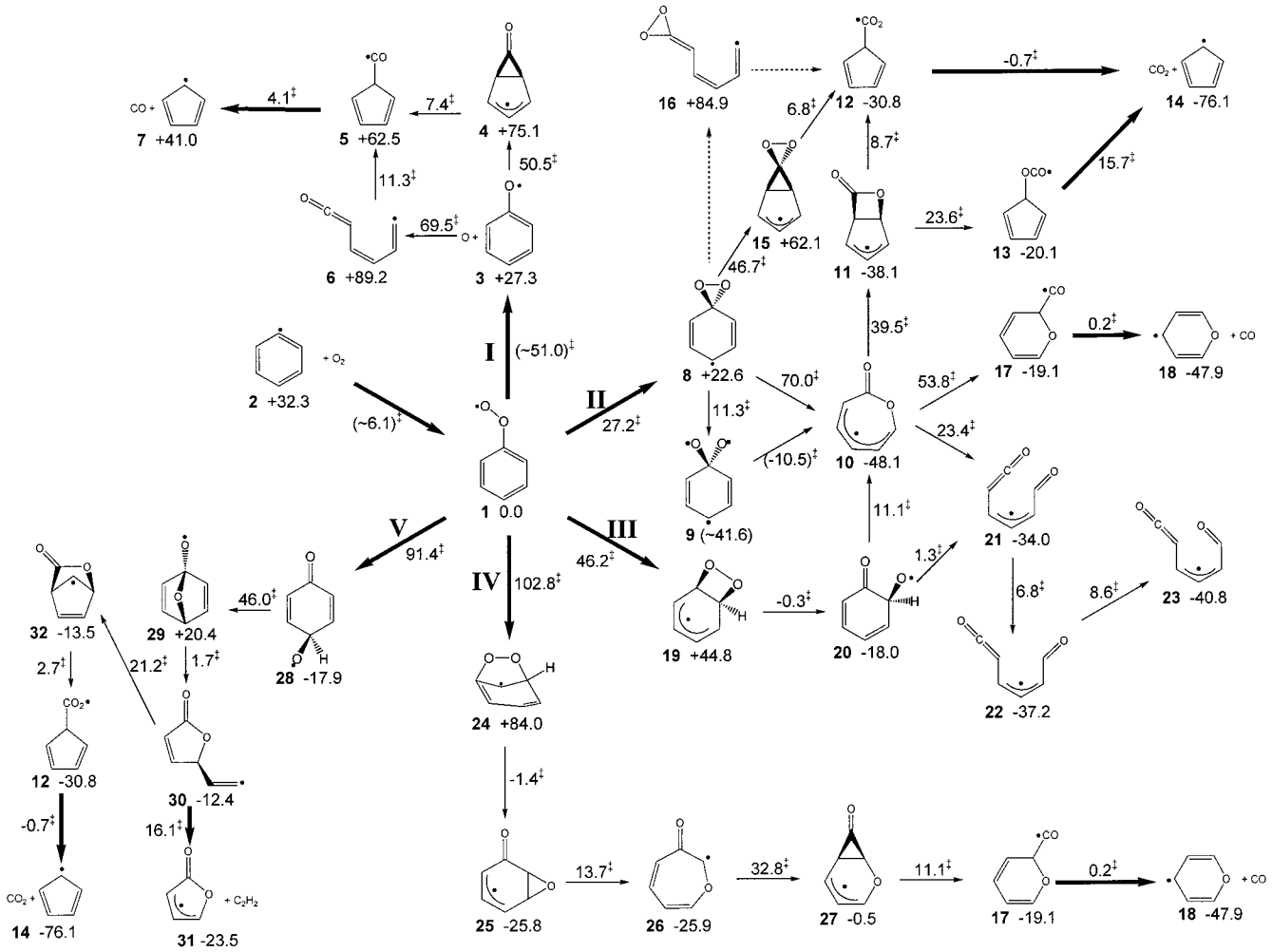

Figure 1. Unimolecular decomposition pathways of phenylperoxy radical. The relative free energies (298 K, kcal/mol) at the B3LYP/6-311+G**//B3LYP/6-31G* level are shown for each intermediate relative to **1**, and each free energy of activation is relative to the reactant for that specific step.

To compare our B3LYP data to other theoretical levels, we have also determined single-point energies at the CASSCF(7,8)/6-31G*, CAS-MP2(7,8)/6-31G*, and UCCSD(T)/6-31G** levels for some key intermediates and transition states.[24−28] The active space for the CASSCF calculations was problematic to determine for the disparate structures, as most of them were of C_1 symmetry. For **1** (C_s symmetry), six orbitals were of π symmetry, and the two chosen σ orbitals had large O−O interactions. For the other structures, the four highest occupied and four lowest unoccupied orbitals were used as obtained from ROHF/6-31G* wave functions. The CASSCF and UCCSD(T) calculations were completed with Gaussian 98.

The stationary points were verified to be minima or saddle points via vibrational frequency analyses. All transition states were confirmed to connect to reactants and products by incrementally displacing (typically 10%) the geometries along the reaction coordinate for the imaginary vibrational frequency in either direction, calculating the analytical force constants, and then optimizing to the corresponding minimum or by using an intrinsic reaction coordinate (IRC) search.[29,30]

Spin contamination throughout this study was very minimal. The $\langle S^2 \rangle$ values for the doublet species (minima and transition states) in this paper were ≤ 0.80, with only six that exceeded 0.80. Three of the six possess minimal spin contamination (**TS 1**−**24**, 0.88; **TS 24**−**25**, 0.84; **TS 1**−**28**, 0.82; Figure 1), while the other three suffer from extreme spin contamination (**TS 1**−**3**, 1.77; **TS 2**−**1**, 1.76; **9**, 1.82), causing the energetics calculated for these molecules to be greatly suspect.

The thermodynamic contribution to the free energy of each molecule was determined from the unscaled vibrational frequencies using the Thermo94 program.[31] The overall Gibbs free energy at each temperature was calculated by adding the single-point energy, the scaled zero-point energy, the thermodynamic contribution to the free energy, and the electronic contribution to the Gibbs free energy. A scaling factor of 0.9806 was used

$$G(T) = E_{SP} + \mathrm{ZPE} + G_{thermo} + RT \ln 2$$

for the ZPE as determined at the B3LYP/6-31G* level.[32] The only molecule which was treated differently was the O atom, where experimentally[33] determined splitting energies were included in the free energy calculations to determine the electronic component of the partition function.

The energies discussed below are free energies computed at B3LYP/6-311+G**//B3LYP/6-31G*, unless noted otherwise. The energies have been evaluated from 298 to 1250 K and will be discussed accordingly in the text.

Results and Discussion

Formation of $C_6H_5OO^{\bullet}$. Formation of $C_6H_5OO^{\bullet}$ (**1**) from the oxidation of phenyl radical with molecular oxygen (**2**) is exoergic at temperatures ranging from 298 to 1000 K and endoergic at temperatures above 1250 K (Table 1). The B3LYP/6-311+G**//B3LYP/6-31G* method calculates this reaction to be favorable by −32.3 kcal/mol at 298 K, decreasing steadily

TABLE 1. Gibbs Free Energy for All Intermediates and Transition States (298−1250 K) at the B3LYP/6-311+G//B3LYP/6-31G* Level**

structure	E^g (hartrees/part)	ΔG(298 K) (kcal/mol)	ΔG(500 K) (kcal/mol)	ΔG(750 K) (kcal/mol)	ΔG(1000 K) (kcal/mol)	ΔG(1250 K) (kcal/mol)	$\langle S^2 \rangle$	other (PG, ES, N_{imag})[h]
1	−382.06960	0.0	0.0	0.0	0.0	0.0	0.76	C_s, $^2A''$, 0
TS 1−3	−381.98196	51.0	49.8	48.3	46.8	45.5	1.77	C_1, 1
TS 1−8	−382.02404	27.2	27.6	28.0	28.6	29.3	0.79	C_1, 1
TS 1−19	−381.99465	46.2	46.9	47.9	49.0	50.2	0.78	C_1, 1
TS 1−24	−381.90221	102.8	103.5	104.3	105.1	106.0	0.88	C_1, 1
TS 1−28	−381.92072	91.4	91.9	92.6	93.3	94.0	0.82	C_1, 1
2[a]	−381.99718	32.3	24.9	15.9	7.1	−1.6	0.76	C_{2v}, $^2A_1$, 0
TS 2−1	−381.99742	38.4	34.9	30.7	26.6	22.6	1.76	C_1, 1
3[b]	−382.00773	27.3	20.6	12.3	3.9	−4.4	0.79	C_s, $^2A''$, 0
TS 3−4b	−381.92354	77.8	71.1	62.8	54.6	46.4	0.77	C_1, 1
TS 3−6b	−381.88861	96.8	88.5	77.9	67.4	57.0	0.77	C_1, 1
4[b]	−381.92831	75.1	68.0	58.9	48.9	40.6	0.77	C_1, 0
TS 4−5b	−381.91606	82.5	75.6	67.1	58.7	50.3	0.77	C_1, 1
5[b]	−381.94726	62.5	54.7	44.6	34.4	24.2	0.75	C_1, 0
TS 5−7b	−381.93812	66.6	58.4	48.1	37.9	27.7	0.76	C_1, 1
6[b]	−381.90079	89.2	80.2	68.7	57.0	45.3	0.77	C_1, 0
TS 6−5b	−381.88335	100.5	92.5	82.3	72.2	62.2	0.78	C_1, 1
7[c]	−381.95912	41.1	25.4	5.9	−13.5	−32.8	0.77	C_{2v}, $^2B_1$, 0
8	−382.03201	22.6	22.8	22.9	22.9	22.9	0.78	C_s, $^2A''$, 0
TS 8−9	−382.01201	33.9	33.9	33.9	34.0	34.2	0.76	C_1, 1
TS 8−10	−381.91393	92.6	91.7	90.4	89.1	87.8	0.78	C_1, 1
TS 8−15	−381.95475	69.3	69.6	69.9	70.2	70.7	0.78	C_1, 1
9	−382.00039	41.6	41.6	41.4	41.1	40.7	1.82	C_1, 0
TS 9−10	−382.01759	31.1	31.5	32.0	32.7	33.4	0.76	C_1, 1
10	−382.14542	−48.1	−48.4	−48.8	−49.2	−49.6	0.78	C_1, 0
TS 10−11	−382.08120	−8.6	−8.3	−7.8	−7.2	−6.5	0.80	C_1, 1
TS 10−17	−382.06345	5.7	5.1	4.5	3.9	3.4	0.75	C_1, 1
TS 10−21	−382.10117	−24.7	−26.4	−28.7	−30.8	−32.8	0.78	C_1, 1
11	−382.13066	−38.1	−37.7	−37.1	−36.6	−36.2	0.78	C_1, 0
TS 11−12	−382.11495	−29.4	−29.1	−28.5	−27.8	−27.0	0.77	C_1, 1
TS 11−13	−382.09064	−14.5	−14.2	−13.8	−13.3	−12.7	0.80	C_1, 1
12	−382.11603	−30.8	−31.3	−32.0	−32.9	−33.7	0.76	C_1, 0
TS 12−14	−382.11593	−31.5	−31.9	−32.2	−32.5	−32.7	0.76	C_1, 1
13	−382.09894	−20.1	−21.0	−22.2	−23.4	−24.6	0.75	C_1, 0
TS 13−14	−382.07261	−4.4	−4.9	−5.5	−6.0	−6.4	0.76	C_1, 1
14[d]	−382.16688	−76.1	−84.6	−95.1	−105.4	−115.6	0.77	C_{2v}, $^2B_1$, 0
15	−381.96804	62.1	62.2	62.3	62.2	62.1	0.77	C_1, 0
TS 15−12	−381.95538	68.9	69.2	69.6	70.0	70.4	0.76	C_1, 1
16	−381.92550	84.9	82.8	79.8	76.7	73.5	0.77	C_1, 0
17	−382.09779	−19.1	−19.9	−20.9	−21.9	−22.9	0.76	C_1, 0
TS 17−18	−382.09552	−18.9	−19.6	−20.5	−21.3	−22.0	0.77	C_1, 1
18[e]	−382.12348	−47.9	−55.6	−65.2	−74.6	−83.9	0.78	C_1, 0
19	−381.99722	44.8	45.2	45.6	46.0	46.3	0.78	C_1, 0
TS 19−20	−381.99633	44.5	45.1	45.8	46.7	47.6	0.80	C_1, 1
20	−382.09519	−18.0	−18.4	−19.1	−19.8	−20.6	0.76	C_1, 0
TS 20−10	−382.07785	−6.9	−6.7	−6.5	−6.1	−5.6	0.77	C_1, 1
TS 20−21	−382.09181	−16.7	−17.0	−17.3	−17.5	−17.7	0.76	C_1, 1
21	−382.11734	−34.0	−36.0	−38.7	−41.4	−44.2	0.78	C_1, 0
TS 21−22	−382.10567	−27.2	−28.8	−30.8	−32.7	−34.5	0.78	C_1, 1
22	−382.12212	−37.2	−39.5	−42.4	−45.5	−48.5	0.78	C_1, 0
TS 22−23	−382.10755	−28.6	−30.3	−32.5	−34.6	−36.6	0.78	C_1, 1
23	−382.12971	−40.8	−42.3	−44.4	−46.5	−48.6	0.77	C_1, 0
24	−381.93351	84.0	84.6	85.2	85.7	86.1	0.79	C_1, 0
TS 24−25	−381.93412	82.6	83.4	84.3	85.3	86.2	0.84	C_1, 1
25	−382.11072	−25.8	−25.5	−25.2	−24.8	−24.5	0.78	C_1, 0
TS 25−26	−382.08708	−12.1	−11.7	−11.1	−10.3	−9.4	0.79	C_1, 1
26	−382.11026	−25.9	−26.2	−26.6	−27.0	−27.4	0.77	C_1, 0
TS 26−27	−382.05548	6.9	7.1	7.3	7.6	7.9	0.77	C_1, 1
27	−382.06854	−0.5	−0.6	−0.9	−1.2	−1.6	0.77	C_1, 0
TS 27−17	−382.04945	10.6	10.6	10.7	10.9	11.1	0.79	C_1, 1
28	−382.09630	−17.9	−18.1	−18.4	−18.8	−19.1	0.75	C_1, 0
TS 28−29	−382.02212	28.1	28.8	29.7	30.6	31.6	0.76	C_1, 1
29	−382.03599	20.4	21.1	21.8	22.4	22.9	0.76	C_1, 0
TS 29−30	−382.03190	22.1	22.9	23.9	25.0	26.1	0.77	C_1, 1
30	−382.08591	−12.4	−13.1	−14.1	−15.2	−16.3	0.76	C_1, 0
TS 30−31	−382.05549	3.7	2.3	0.4	−1.6	−3.5	0.78	C_1, 1
TS 30−32	−382.05363	8.8	9.4	10.3	11.2	12.2	0.79	C_1, 1
31[f]	−382.08322	−23.5	−31.4	−41.3	−51.2	−61.0	0.77	C_1, 0
32	−382.09249	−13.5	−12.7	−11.6	−10.6	−9.6	0.75	C_1, 0
TS 32−12	−382.08620	−10.8	−10.0	−8.9	−7.7	−6.4	0.76	C_1, 1

[a] Energies include the aryl species and O_2; $\langle S^2 \rangle$ values and symmetry are of the aryl species only. [b] Energies include the aryl species and O; $\langle S^2 \rangle$ values and symmetry are of the aryl species only. [c] Energies include the aryl species, O, and CO; $\langle S^2 \rangle$ values and symmetry are of the aryl species only. [d] Energies include the aryl species and CO_2; $\langle S^2 \rangle$ values and symmetry are of the aryl species only. [e] Energies include the aryl species and CO; $\langle S^2 \rangle$ values and symmetry are of the aryl species only. [f] Energies include the aryl species and acetylene; $\langle S^2 \rangle$ values and symmetry are of the aryl species only. [g] Bottom-of-the-well energy. [h] Point group (PG), electronic state (ES), number of imaginary vibrational frequencies (N_{imag}).

to only −7.1 kcal/mol at 1000 K and becoming unfavorable by +1.6 kcal/mol at 1250 K. The transition state (**TS 2−1**) for this reaction has been found, but suffers from excessive spin contamination ($\langle S^2 \rangle = 1.76$). This is not surprising, since the

reactants are a doublet **2** and a triplet O_2, which produce a doublet **1**. The energy values for the activation barrier predict a $\Delta G^{\ddagger}$(298 K) of 6.1 kcal/mol, which increases steadily to a $\Delta G^{\ddagger}$(1250 K) of 24.2 kcal/mol. The bottom-of-the-well energy value of phenyl radical and O_2 compared to the analogous value of **TS 2−1** differs by only 0.1 kcal/mol. The activation barriers are higher than expected when compared to the related vinyl peroxy radical formation in which the reaction has been reported to be barrierless at temperatures ranging from 299 to 1005 K.[10,34] This discrepancy is probably due to the spin contamination.

The unimolecular decomposition of the phenylperoxy radical (**1**) was explored along five pathways, denoted by the formation of the subsequent intermediates: phenoxy radical (**3**) [path I]; dioxiranyl radical (**8**) [path II]; 1,2-dioxetanyl radical (**19**) [path III]; 1,3-peroxy radical (**24**) [path IV]; and *p*-phenylquinone radical (**28**) [path V]. A complete summary of all the intermediates included in this study is presented in Table 1, and a reaction scheme is shown in Figure 1. It can be seen that the formation of the final products of Cp•, O, and CO; Cp• and CO_2; pyranyl radical (**18**) and CO; oxyfuranyl radical (**31**) and acetylene; or an acyclic $C_6H_5O_2$• species (**23**) is complicated, and several of the products can arise from more than one initial pathway. Experimentally, each of these products, except **23** and **31**, has been detected by mass spectrometric studies during benzene oxidation in a microjet reactor at temperatures from 800 to 1300 K.[35] The absence of **23** and **31** in these experimental results may be due to their facile fragmentation or further decomposition.

In Figure 1, the relative free energies (298 K) at the B3LYP/6-311+G**//B3LYP/6-31G* level are shown for each intermediate relative to phenylperoxy radical (**1**) as 0 kcal/mol. For each step, the free energy of activation ($\Delta G^{\ddagger}$(298 K)) is listed relative to the reactant for that specific step. Activation barriers and intermediates which are considered to be suspect (due to spin contamination issues) are shown in parentheses. Table 1 lists the relative free energies of all stationary points at different temperatures.

Path I. Phenoxy Radical Intermediate. The phenoxy radical (**3**) can possibly be produced from the direct reaction of phenyl radical with O_2 to form **3** or from the homolysis of the O−O bond in phenylperoxy radical (**1**). The first reaction is exoergic by approximately −3 to −5 kcal/mol across the temperature range of 298−1250 K. On the other hand, the scission of the O−O bond from phenylperoxy radical is endoergic by +27.3 kcal/mol at 298 K, decreases to +3.9 kcal/mol at 1000 K, and becomes exoergic by −4.4 kcal/mol at 1250 K. We have attempted to find transition states for both pathways, but without success at the B3LYP/6-31G* level for the first route, and obtained an energy value (51.0 kcal/mol) which is unreliable because of excessive spin contamination for the second route.

We therefore continued to examine the pathways available to the phenoxy radical. Computational exploration of the decomposition pathways of phenoxy radical that were first proposed by Colussi et al.[3] and a subset of the pathways explored by Morokuma et al.[12] yielded results that correlate well with the available experimental and computational data.[3,12,36] For the decomposition of phenoxy radical to Cp• and CO, it is possible for a bicyclic radical (**4**) to be formed or for the ring to open and then form a ketenyl radical species (**6**). As expected, the formation of **4** is more favorable and has an activation barrier that is ∼19 kcal/mol (298 K) lower than the activation barrier to form **6**. Furthermore, the bicyclic intermediate **4** is ∼14.1 kcal/mol more stable than **6** at 298 K. The next step is the formation of **5**. This occurs either through the cyclopropyl ring opening of **4** or via a ring closure of **6**. The activation barrier for the most favorable pathway (**4** → **5**) is 7.4 kcal/mol (298 K). For comparison to previous results, our stepwise bottom-of-the-well energies with scaled ZPE corrections at the B3LYP/6-311+G**//B3LYP/6-31G* level are similar to the values calculated by Morokuma et al.[12] at the G2M(rcc,MP2) level for similar structures, such as **TS 3−4** and **TS 4−5**. Our activation barriers are 50.5 and 55.3 kcal/mol, which compare to calculated G2M(rcc,MP2) values of 48.9 and 51.9 kcal/mol,[12] respectively. The final step is the simple decomposition of **5** to yield Cp• and CO as products.

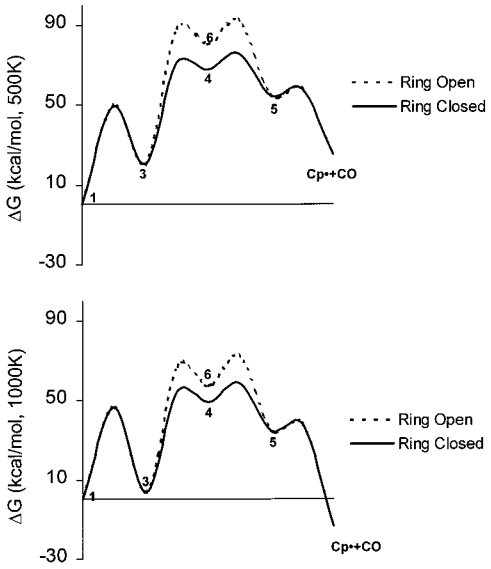

Figure 2. Unimolecular decomposition (500 K, top, and 1000 K, bottom) of phenylperoxy radical to yield Cp• + CO + O via a phenoxy radical intermediate (path I) at the B3LYP/6-311+G**//B3LYP/6-31G* level. See Figure 1 for structures.

Overall, the activation barrier in the initial step of **3** → **4** is calculated to be ∼51 kcal/mol at all temperatures evaluated. This is similar to the experimentally determined activation energy of 44.0 ± 0.9 kcal/mol at 1000−1580 K.[36] Using simple transition-state theory[37] for the calculated free energies of activation along the lowest energy pathway, **3** → **4** → **5**, the overall reaction rate for the decomposition of phenoxy radical to Cp• and CO is 20 s^{-1} at 1000 K, which compares to experimentally determined values of 10 ± 5 s^{-1} (1000 K)[3] and 63.4 s^{-1}.[36,38]

At all temperatures studied here, the reaction pathway which proceeds through the nonplanar bicyclic radical (**4**) is lower in energy, as shown in Figure 2. However, it is interesting to note that the energy gap between the two pathways steadily decreases with increasing temperature, and at temperatures greater than ∼2200 K, the ring opening pathway yielding the ketenyl radical intermediate (**6**) will be the more favorable.

Path II. Dioxiranyl Radical Intermediate. The dioxiranyl radical (**8**) is formed by a ring closure (1,1-addition) of the terminal oxygen of phenylperoxy radical (**1**) onto the phenyl ring. The activation barrier for this rearrangement (**1** → **8**) is 27.2 kcal/mol at 298 K, which is very similar (∼0.1 kcal/mol) to the relative free energy of formation of phenoxy radical and an oxygen atom (**1** → **3**). At temperatures ≥430 K, the overall free energy for the **1** → **3** pathway attains greater stability than the initial step of the dioxiranyl radical pathway.

Subsequent decomposition of the dioxiranyl radical (**8**) can possibly occur along two distinct pathways. The first pathway, proposed originally by Carpenter,[7] involves rearrangement to

form a seven-membered ring intermediate (**10**). An alternate pathway occurs via cyclization of **8** to form **15** in a step that is analogous to **3** → **4** in the phenoxy radical decomposition.

The first step along Carpenter's proposed pathway is the isomerization of **8** to yield the seven-membered ring **10**. Carpenter calculated, using the PM3 method, that the $\Delta H^{\ddagger}$ for this reaction is 10.5 kcal/mol (298 K) with an overall exothermicity of −74.5 kcal/mol. Correlations between these results and those obtained at the B3LYP level are good, but require the inclusion of the intermediate **9** in the reaction step. With this addition, the B3LYP method calculates the overall activation barrier to this isomerization to be 11.3 kcal/mol (298 K) with an overall exoergicity (**8** → **9** → **10**) of −70.7 kcal/mol. A direct transition state to form **10** from **8** also exists, but the activation barrier is very high (70.0 kcal/mol).

The stepwise isomerization (**8** → **9** → **10**) begins with the scission of the O−O bond of **8**. This reaction has an activation barrier of 11.3 kcal/mol (298 K) and results in the intermediate **9**. Structure **9** can exist as a doublet or quartet as shown by Mebel and Lin,[13] and the doublet state should be more stable. The energy for this intermediate, as calculated with the B3LYP method, is greater than the energy of the transition state leading to its formation from **8** or the energy of the transition state proceeding from **9** to **10**. This is a result of excessive spin contamination in **9**, but the transition states (**TS 8**−**9** and **TS 9**−**10**) do not suffer from this problem. The activation barrier for **9** → **10** is lower in Gibbs free energy at all temperatures studied than the activation barrier for the O−O bond scission. Therefore, the scission of the O−O bond is the greatest barrier (11.3 kcal/mol) for the isomerization of **8** to yield the seven-membered ring **10**.

Structure **10** can then isomerize to form the nonplanar bicyclic radical (**11**), the pyranyl species (**17**), or the acyclic structure (**21**). The lowest activation barrier for the rearrangement of **10** at 298 K, 23.4 kcal/mol, leads to the formation of **21**, followed by the isomerization to **11** (39.5 kcal/mol) and then the production of **17** with a barrier of 53.8 kcal/mol. These values are similar to the enthalpic barriers that Carpenter[7] calculated of 30.0 and 37.0 kcal/mol, leading to the first two intermediates (**21** and **11**, respectively). Carbon dioxide is readily extruded from **11** with an activation barrier of 8.7 kcal/mol via the **11** → **12** → **14** pathway to yield Cp• and CO_2. The simple decomposition of **17** to the pyranyl radical (**18**) and CO is essentially barrierless at all temperatures. (Please note that the relative free energies for **12** → **14** in this paper differ from our earlier results on the dioxiranyl pathway in phenylperoxy radical and is due to a previously undetected spreadsheet error for CO_2 in Figure 3 of ref 8. The exoergicity for **12** → **14** is −45.3 kcal/mol.)

An alternate pathway in the unimolecular decomposition of the dioxiranyl radical is via a mechanism similar to the phenoxy radical decomposition to generate Cp• and CO. The formation of a nonplanar tricyclic radical (**15**) is rather endoergic, but surprisingly not as much as for the formation of the bicyclic radical (**4**) along the phenoxy radical pathway. At 298 K, the activation barrier is 46.7 kcal/mol to create **15**. Simple decomposition of **15** to Cp• and CO_2 will occur readily with an activation barrier of only ∼6.8 kcal/mol, resulting in an overall exoergic reaction of −138.2 kcal/mol (298 K) from **15**.

Ring opening of **8** to generate **16** as the product is expected to be a higher energy pathway. Structure **16** is higher in energy by ∼15 kcal/mol than the transition state to form **15**; however, we have not searched for the corresponding transition state to form **16**, but once again, it appears from the energetic trends

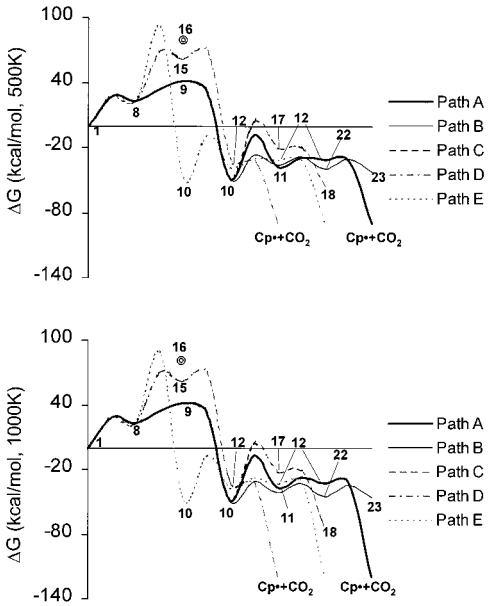

Figure 3. Unimolecular decomposition (500 K, top, and 1000 K, bottom) of phenylperoxy radical to Cp• + CO_2, Py• (**18**) + CO, or an acyclic species (**23**) via a 1,1-dioxiranyl radical intermediate (path II) at the B3LYP/6-311+G**//B3LYP/6-31G* level. See Figure 1 for structures. Path A = **1**−**8**−**9**−**10**−**11**−**12**−**Cp•** + **CO_2**. Path B = **1**−**8**−**9**−**10**−**21**−**22**−**23**. Path C = **1**−**8**−**9**−**10**−**17**−**18**. Path D = **1**−**8**−**15**−**12**−**Cp•** + **CO_2**. Path E = **1**−**8**−**10**−**11**−**12**−**Cp•** + **CO_2**.

that opening of the ring will be favored over the formation of the tricyclic radical intermediate (**15**) at high temperatures.

At all temperatures evaluated (Figure 3), it appears that the energetically most favored pathway for the decomposition of the dioxiranyl radical (**8**) is the one that is analogous to the Carpenter pathway, i.e. **8** → **9** → **10** → **14**, **18**, or **23**.

Path III. 1,2-Dioxetanyl Radical Intermediate. The formation of a 1,2-dioxetanyl intermediate (**19**) is endoergic by +44.8 kcal/mol with a free energy of activation of 46.2 kcal/mol at 298 K. Both the activation barrier and ground-state free energy of **19** increase gradually with increasing temperature, and at 1250 K, the energies are 50.2 and 46.3 kcal/mol, respectively. The isomerization of **19** to form the *o*-phenylquinone radical (**20**) is essentially barrierless at temperatures <500 K and remains below 2 kcal/mol at temperatures above 1250 K. The isomerization of **20** can proceed either through an epoxide-like transition state (**TS 20**−**10**) to yield the seven-membered ring (**10**) or through a scission of the C_1−C_2 bond, producing the acyclic structure **21**. Contrary to the phenoxy and dioxiranyl radical pathways, the ring-opening mechanism is the lowest energy pathway for the unimolecular rearrangement of **20**, and the energy gap between the stability of the two transition states (**TS 20**−**10** and **TS 20**−**21**) only increases with temperature. If **10** and **21** are produced, they can decompose in the same manner as described in path II, resulting in Cp• and CO_2, pyranyl radical (**18**) and CO, or the acyclic ketenyl radical structure (**23**). The ring-opening pathway appears to be the optimum pathway at all temperatures for the decomposition of phenylperoxy radical if it proceeds through a 1,2-dioxetanyl intermediate (Figure 4).

Path IV. 1,3-Peroxy Radical Intermediate. The isomerization of phenylperoxy radical (**1**) to form a 1,3-peroxy radical (**24**) requires a tremendous amount of energy. Not only does this intermediate lose aromaticity, but it also results in a bicyclic, anti-Bredt[39] alkene that cannot stabilize the radical. The energy barrier for the production of **24** at 298 K exceeds 102 kcal/mol and only increases with increasing temperature. Thus, if

TABLE 2. Relative Energies (kcal/mol) at Different Theoretical Levels for a Few Important Intermediates and Transition States[a]

	1	**TS 1−8**	**8**	**TS 8−9**	**9**	**TS 9−10**	**10**	**TS 10−11**	**11**
CASSCF(7,8)/6-31G*	0.0	17.1	4.7	9.0	45.4	26.5	−36.9	−16.7	−59.7
CAS-MP2(7,8)/6-31G*	0.0	36.9	31.7	40.5	61.5	53.0	−63.8	−8.6	−57.9
UMP2/6-31G**	0.0	47.5	28.3	50.7	67.2	55.5	−32.9	2.5	−44.1
UMP3/6-31G**	0.0	40.5	25.2	51.4	47.1	59.5	−37.5	0.2	−43.5
UMP4(SDQ)/6-31G**	0.0	36.6	21.4	43.6	45.5	52.0	−42.0	−4.9	−47.3
UCCSD/6-31G**	0.0	29.0	18.3	39.5	40.0[b]	54.1[b]	−45.8	−9.2	−45.9
UCCSD(T)/6-31G**	0.0	28.4	19.1	34.6	[b]	[b]	−43.6	−8.6	−43.6
UB3LYP/6-31G*	0.0	28.4	22.8	39.8	46.2	37.1	−45.9	−4.9	−36.7
UB3LYP/6-311+G**	0.0	28.6	23.6	36.1	43.4	32.6	−47.6	−7.3	−38.3
UB3LYP/6-311+G** $\langle S^2\rangle$	0.76	0.79	0.79	0.76	1.82	0.76	0.78	0.80	0.78
UCCSD(T)/6-31G** $\langle S^2\rangle$	0.77	1.42	1.21	1.20	2.24	0.76	1.27	1.36	0.97

[a] The B3LYP/6-31G* geometry was used in each case. [b] The CCSD equations could not be converged to the necessary accuracy ($<10^{-7}$ au) by Gaussian 98 to complete the UCCSD(T) calculation. The corresponding CCSD energies for **9** and **TS 9−10** reflect a 10^{-5} au convergence.

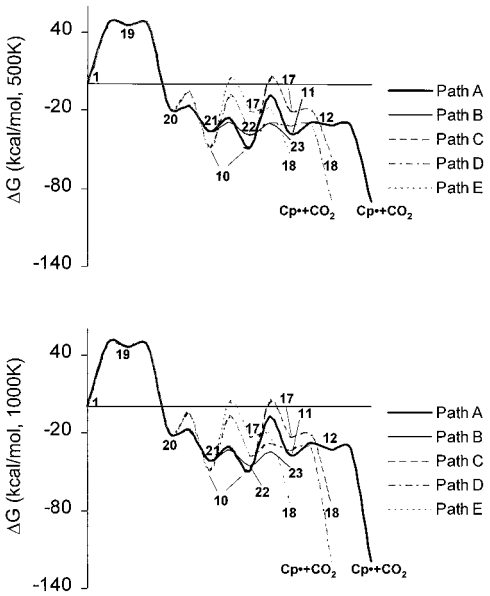

Figure 4. Unimolecular decomposition (500 K, top, and 1000 K, bottom) of phenylperoxy radical to Cp$^\bullet$ + CO_2, Py$^\bullet$ (**18**) + CO, or an open ring species via a 1,2-dioxetanyl radical intermediate (path III) at the B3LYP/6-311+G**//B3LYP/6-31G* level. See Figure 1 for structures. Path A = **1−19−20−21−10−11−12−Cp$^\bullet$ + CO_2**. Path B = **1−19−20 −21−22−23**. Path C = **1−19−20−21−10−17−18**. Path D = **1−19−20−10−11−12−Cp$^\bullet$ + CO_2**. Path E = **1−19−20 −10−17−18**.

phenylperoxy radical is able to gain enough internal energy to isomerize to structure **24**, the final products of pyranyl radical (**18**) and CO are much lower in energy.

The first step is the formation of an epoxide species (**25**) which can then rearrange to form **26**, which is an isomer of the stable seven-membered ring intermediate (**10**) along the dioxiranyl radical pathway. The two structures (**25** and **26**) are very similar in ground-state energies at 298 K, but as the temperature increases, intermediate **26** gains moderately in stability as compared to **25**. Structure **26** can then close the ring to form a nonplanar bicyclic radical (**27**), which is slightly more stable than the phenylperoxy radical at all temperatures. The activation energy for this process is 32.8 kcal/mol (298 K) and is the highest barrier along this pathway after the costly initial step to form **24**. Structure **27** can then lose CO to yield the final pyranyl radical (**18**) product.

Path V. *p*-Phenylquinone Radical Intermediate. Another pathway that was explored, but is highly improbable, is the transformation of the phenylperoxy radical to *p*-phenylquinone radical (**28**) via a 1,4-addition. The free energy of activation for this reaction is 91.4 kcal/mol at 298 K and steadily rises to 94.0 kcal/mol at 1250 K; however, the overall reaction is exoergic by −17.9 to −19.1 kcal/mol throughout the same temperature range. The pathway explored from this point was chosen to provide an alternate mechanism for the production of Cp$^\bullet$. The *p*-phenylquinone radical (**28**) incurs a significant energetic penalty to form the bicyclic radical structure (**29**), which can then break open the ring to form the stable intermediate **30**.

Structure **30** can than rearrange in two different ways. The lowest energy pathway yields acetylene and a γ-lactone radical (**31**). The other possibility is an isomerization that results in another bicyclic radical (**32**) which leads to CO_2 extrusion and the formation of Cp$^\bullet$. The key transition states at the diverging point are **TS 30−31** and **TS 30−32**. As the temperature increases, the stability of **TS 30−31** is favored, thereby increasing the relative activation barrier gap—further promoting the production of **31**.

Comparison of Theoretical Methods. To evaluate the quantitative accuracy of the B3LYP energies, we have also calculated single-point energies at the CASSCF(7,8)/6-31G*, CAS-MP2(7,8)/6-31G*, and UCCSD(T)/6-31G** levels for some key intermediates and transition states. These relative energies (at the bottom of the well) are provided in Table 2. The CASSCF calculations are problematic due to the choice of the active space for these diverse structures. As seen in Table 2, there is a lack of convergence between the CASSCF energies and the other methods, and is most likely due to the choice of the active space. A correct treatment of this system by CASSCF methods will require a more extensive analysis.

However, for comparison to the B3LYP energies, we have also calculated UCCSD(T)/6-31G** single-point energies, and these are also shown in Table 2. The UCCSD(T) energies are in good qualitative and quantitative agreement with the B3LYP results, except for structures **9** and **TS 9−10**, which have spin contamination and/or UCCSD(T) convergence problems.

Comparison of Reaction Pathways at Different Temperatures. In comparing the lowest energy mechanism for each pathway that leads to Cp$^\bullet$ production, the 1,1-dioxiranyl radical pathway appears to be the most favored pathway from 298 to 1250 K on the basis of the lowest overall activation barrier, **TS 8−9** (Figure 5). When the largest cumulative activation barrier is considered, the 1,2-dioxetanyl radical pathway (via **TS 1−19**) is even more favorable than the phenoxy radical pathway (via **TS 4−5**) from 298 to 750 K, but is significantly less available than the 1,1-dioxiranyl radical pathway. As the temperature increases to 1000 K, the phenoxy radical decomposition pathway's overall activation barrier decreases to where it is roughly equivalent to the 1,2-dioxetanyl radical pathway, and by 1250 K, the phenoxy radical pathway (path I) is becoming

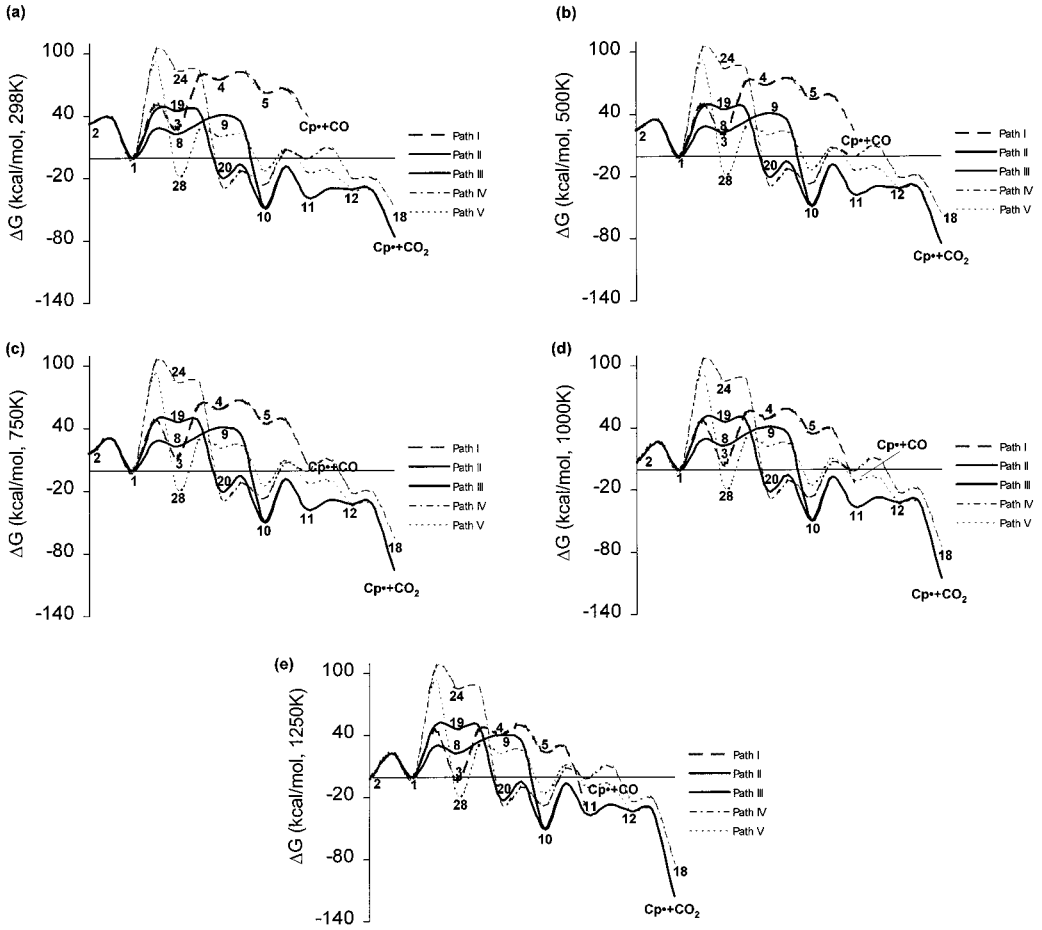

Figure 5. Unimolecular decomposition of phenylperoxy radical to Cp• + CO + O, Cp• + CO_2, or Py• (**18**) + CO from 298 (a), 500 (b), 750 (c), 1000 (d), and 1250 (e) K at the B3LYP/6-311+G**//B3LYP/6-31G* level. See Figure 1 for structures.

competitive with the 1,1-dioxiranyl radical pathway as the barriers along path I become more accessible (Figure 5).

This comparison neglects that the lowest energy route along the 1,1-dioxiranyl pathway (via **8** → **9** → **10** → **21** → **22** → **23)** yields the acyclic species **23**. Therefore, decomposition of the phenylperoxy radical (**1**) at low to intermediate temperatures (<1250 K) should produce greater amounts of products from a ring-opened structure than the production of Cp•. Such ring-opened products (or fragments thereof) have been seen experimentally.[35]

The reaction mechanisms have been compared at varying temperatures which are relevant to atmospheric or combustion processes. This potential energy surface will serve as a model for further research of oxidation pathways for heteroaromatic radicals that are relevant to coal. Further study in determining the overall reaction rates for each pathway is needed to fully confirm these conclusions, and these studies will be presented in due course.

Acknowledgment. We gratefully acknowledge the U.S. Department of Energy (Grant DE-FG22-96PC96249), the U.S. Army, and the Ohio Supercomputer Center for support of this research. We thank Paul R. Rablen (Swarthmore College) for providing his Thermo94 program.

Supporting Information Available: Energies, enthalpies, and free energies as a function of temperature for all intermediates and transition states for the reaction of phenyl radical with O_2 and the subsequent rearrangement pathways of phenylperoxy radical, and Cartesian coordinates (Å) and harmonic vibrational frequencies (cm^{-1}) for all intermediates and transition states for the reaction of phenyl radical with O_2 and the subsequent rearrangement pathways of phenylperoxy radical. This material is available free of charge via the Internet at http://pubs.acs.org.

References and Notes

(1) Brezinsky, K. *Prog. Energy Combust. Sci.* **1986**, *12*, 1−24.
(2) Bittker, D. A. *Combust. Sci. Technol*. **1991**, *79*, 49−72.
(3) Colussi, A. J.; Zabel, F.; Benson, S. W. *Int. J. Chem. Kinet*. **1977**, *9*, 161−178.
(4) Zhang, H.-Y.; McKinnon, J. T. *Combust. Sci. Technol*. **1995**, *107*, 261−300.
(5) Benson, S. W. *J. Am. Chem. Soc*. **1965**, *87*, 972.
(6) Yu, T.; Lin, M. C. *J. Am. Chem. Soc*. **1994**, *116*, 9571−9576.
(7) Carpenter, B. K. *J. Am. Chem. Soc*. **1993**, *113*, 9806−9807.
(8) Barckholtz, C.; Fadden, M. J.; Hadad, C. M. *J. Phys. Chem. A* **1999**, *103*, 8108−8117.
(9) Carpenter, B. K. *J. Phys. Chem.* **1995**, *99*, 9801−9810.
(10) Mebel, A. M.; Diau, E. W. G.; Lin, M. C.; Morokuma, K. *J. Am. Chem. Soc.* **1996**, *118*, 9759−9771.
(11) Olivella, S.; Sole, A.; Garcia-Raso, A. *J. Phys. Chem.* **1995**, *99*, 10549.
(12) Liu, R.; Morokuma, K.; Mebel, A. M.; Lin, M. C. *J. Phys. Chem.* **1996**, *100*, 9314−9322.
(13) Mebel, A. M.; Lin, M. C. *J. Am. Chem. Soc.* **1994**, *116*, 9577−9584.
(14) Lin, M. C.; Mebel, A. M. *J. Phys. Org. Chem.* **1995**, *8*, 407−420.
(15) Mebel, A. M.; Lin, M. C.; Yu, T.; Morokuma, K. *J. Phys. Chem. A* **1997**, *101*, 3189−3196.
(16) Barckholtz, C.; Barckholtz, T. A.; Hadad, C. M. *J. Am. Chem. Soc.* **1999**, *121*, 491−500.
(17) Frisch, M. J.; Trucks, G. W.; Schlegel, H. B.; Gill, P. M. W.; Johnson, B. G.; Robb, M. A.; Cheeseman, J. R.; Keith, T.; Petersson, G. A.; Montgomery, J. A.; Raghavachari, K.; Al-Laham, M. A.; Zakrzewski, V. G.; Ortiz, J. V.; Foresman, J. B.; Peng, C. Y.; Ayala, P. Y.; Chen, W.; Wong, M. W.; Andres, J. L.; Replogle, E. S.; Gomperts, R.; Martin, R. L.;

Fox, D. J.; Binkley, J. S.; Defrees, D. J.; Baker, J.; Stewart, J. J. P.; Head-Gordon, M.; Gonzalez, C.; Pople, J. A. Gaussian 94, Revision D.3; Gaussian, Inc.: Pittsburgh, PA, 1995.

(18) Frisch, M. J.; Trucks, G. W.; Schlegel, H. B.; Scuseria, G. E.; Robb, M. A.; Cheeseman, J. R.; Zakrzewski, V. G.; Montgomery, J. A., Jr.; Stratmann, R. E.; Burant, J. C.; Dapprich, S.; Millam, J. M.; Daniels, A. D.; Kudin, K. N.; Strain, M. C.; Farkas, O.; Tomasi, J.; Barone, V.; Cossi, M.; Cammi, R.; Mennucci, B.; Pomelli, C.; Adamo, C.; Clifford, S.; Ochterski, J.; Petersson, G. A.; Ayala, P. Y.; Cui, Q.; Morokuma, K.; Malick, D. K.; Rabuck, A. D.; Raghavachari, K.; Foresman, J. B.; Cioslowski, J.; Ortiz, J. V.; Stefanov, B. B.; Liu, G.; Liashenko, A.; Piskorz, P.; Komaromi, I.; Gomperts, R.; Martin, R. L.; Fox, D. J.; Keith, T.; Al-Laham, M. A.; Peng, C. Y.; Nanayakkara, A.; Gonzalez, C.; Challacombe, M.; Gill, P. M. W.; Johnson, B.; Chen, W.; Wong, M. W.; Andres, J. L.; Gonzalez, C.; Head-Gordon, M.; Replogle, E. S.; Pople, J. A. Gaussian 98, Revision A.6; Gaussian, Inc.: Pittsburgh, PA, 1998.

(19) Becke, A. D. *Phys. Rev. A* **1988**, *38*, 3098−3100.

(20) Lee, C.; Yang, W.; Parr, R. G. *Phys. Rev. B* **1988**, *37*, 785−789.

(21) Becke, A. D. *J. Chem. Phys.* **1993**, *98*, 1372.

(22) Hehre, W. J.; Radom, L.; Schleyer, P. v. R.; Pople, J. A. *Ab Initio Molecular Orbital Theory*; John Wiley & Sons: New York, 1986

(23) Bauschlicher, C. W., Jr.; Langhoff, S. R. *Mol. Phys.* **1999**, *96*, 471.

(24) Hegarty, D.; Robb, M. A. *Mol. Phys.* **1979**, *38*, 1795.

(25) Eade, R. H.; Robb, M. A. *Chem. Phys. Lett.* **1981**, *83*, 362.

(26) Schlegel, H. B.; Robb, M. A. *Chem. Phys. Lett.* **1982**, *93*, 43.

(27) Yamamoto, N.; Vreven, T.; Robb, M. A.; Frisch, M. J.; Schlegel, H. B. *Chem. Phys. Lett.* **1996**, *250*, 373.

(28) Stanton, J. F.; Gauss, J.; Watts, J. D.; Lauderdale, W. J.; Bartlett, R. J. *Int. J. Quantum Chem.* **1992**, *S26*, 879.

(29) Gonzalez, C.; Schlegel, H. B. *J. Chem. Phys.* **1989**, *90*, 2154.

(30) Gonzalez, C.; Schlegel, H. B. *J. Phys. Chem.* **1990**, *94*, 5523.

(31) Rablen, P. R., Thermo94. Yale University, 1994.

(32) Scott, A. P.; Radom, L. *J. Phys. Chem*. **1996**, *100*, 16502−16513.

(33) Chase, M. W., Jr. *NIST-JANAF Thermochemical Tables*; American Chemical Society: Washing, DC; American Institute of Physics for the National Institute of Standards and Technology: New York, 1998.

(34) Knyazev, V. D.; Slagle, I. R. *J. Phys. Chem*. **1995**, *99*, 2247−2249.

(35) Chai, Y.; Pfefferle, L. D. *Fuel* **1998**, *77*, 313−320.

(36) Lin, C.-Y.; Lin, M. C. *J. Phys. Chem*. **1986**, *90*, 425−431.

(37) The calculated kinetic treatment was performed as discussed in ref 3.

(38) The expression listed in the paper (ref 28) is $10^{11.90\pm0.20}$ $\exp(-23900 \pm 450/T)$ s^{-1}, and corresponds to a range of 25.5−157.6 s^{-1}, on the basis of the published error bars.

(39) Bredt, J.; Thouet, H.; Schmitz, J. *Liebigs Ann. Chem.* **1924**, 437, 1.